View Online / Journal Homepage / Table of Contents for this issue
Dynamic Article Links

Soft Matter

Cite this: *Soft Matter*, 2011, **7**, 10631

www.rsc.org/softmatter

PAPER

Self-organized patterns of actin filaments in cell-sized confinement†

Marina Soares e Silva, José Alvarado, Jeanette Nguyen, Nefeli Georgoulia,‡ Bela M. Mulder and Gijsje H. Koenderink*

Received 7th June 2011, Accepted 1st September 2011
DOI: 10.1039/c1sm06060k

Cells use actin filaments to define and maintain their shape and to exert forces on the surrounding tissue. Accessory proteins like crosslinkers and motors organize these filaments into functional structures. However, physical effects also influence filament organization: steric interactions impose packing constraints at high filament density and spatially confine the filaments within the cell boundaries. Here we investigate the combined effects of packing constraints and spatial confinement by growing dense actin networks in cell-sized microchambers with nonadhesive walls. We show that the filaments spontaneously form dense, bundle-like structures above a threshold concentration of 1 mg ml^{-1}, in contrast to unconfined networks, which are homogeneous and undergo a bulk isotropic-to-nematic phase transition above 5 mg ml^{-1}. Bundling requires quasi-2D confinement in chambers with a depth comparable to the mean filament length (6 μm). The bundles curve along the walls and central bundles align along the chamber diagonal or, in elongated chambers, along the long axis. We propose that bundling is a result of the polydisperse length distribution of the filaments: filaments shorter than the chamber depth introduce an entropic depletion attraction between the longest filaments, which are confined in-plane. Bundle alignment reflects a competition between bulk liquid-crystalline ordering and alignment along the boundaries. This physical mechanism may influence intracellular organization of actin in combination with biochemical regulation and actin–membrane adhesion.

Introduction

The shape and internal organization of eukaryotic cells are governed by a complex and dynamic network of filamentous proteins known as the cytoskeleton. The backbone of this cytoskeleton is formed by three types of long and stiff biopolymers: microtubules, actin filaments, and intermediate filaments. The spatial arrangement of these filaments is regulated by a large set of accessory proteins that crosslink the cytoskeletal filaments to each other[1] and to the cell membrane.[2] Moreover, the cytoskeleton is actively remodeled by processes that use metabolic energy, such as filament (de-)polymerization and sliding by motor proteins.[3] This biochemical regulation inevitably operates under constraints set by physical effects.

An important physical constraint is provided by the finite size of cells and their internal compartments. The typical size of eukaryotic cells ranges from ~10 μm for yeast cells to ~50 μm for plant and animal cells.[4] In plants, the cytoplasm is in many parts of the cell confined within a thin layer of only 1 μm that is sandwiched between the rigid cell wall and the vacuole, which takes up nearly 90% of the cytoplasmic space.[5] In animal cells, the cytoplasm is usually more three-dimensional and is bounded by a lipid bilayer membrane which is soft and deformable. However, many types of animal cells bear a rigid extracellular polymer layer anchored to the cell membrane known as the pericellular coat[6,7] and in epithelial tissues, membrane fluctuations are constrained by close packing of the cells and active tension imposed by the actin–myosin cytoskeleton.[8] Furthermore, certain regions of the cytoskeleton are often tightly confined in thin cell extensions. Migrating cells advance with sheet-like lamellipodia with heights of only 0.1–0.2 μm, filled with a dense meshwork of actin.[9–11] Cells also generate long and thin membrane protrusions filled with actin or microtubules, such as filopodia, stereocilia, and neurite processes.[12] Since actin filaments and microtubules are rather rigid on these cellular scales, we expect that geometrical constraints are relevant for their organization *in vivo*. However, the inherent complexity of cells hampers a clear distinction between the effect of confinement and that of regulatory proteins.

Several experimental studies have isolated the influence of confinement on cytoskeletal organization by reconstituting purified actin or tubulin in cell-sized liposomes, emulsion droplets, or microfabricated chambers. Long cytoskeletal filaments

FOM Institute AMOLF, 1009 DB Amsterdam, Netherlands. E-mail: g.koenderink@amolf.nl

† Electronic supplementary information (ESI) available: Materials and methods (protein purification, microchamber fabrication, actin length measurements, image analysis methodology) and figures to support observations reported in the main text (image analysis examples, statistical tests, additional bundle parameter data). See DOI: 10.1039/c1sm06060k

‡ Current address: Harvard Medical School, Boston MA, USA.

confined in small containers with rigid walls have to bend, and the associated energy penalty forces them to align close to the walls.[13–15] Filaments inside liposomes, however, can avoid bending by generating membrane protrusions, provided that the force resisting protrusion does not exceed the Euler buckling force. Microtubules, which have millimetre persistence lengths, have been shown to generate protrusions in the absence of crosslinkers,[16–19] whereas actin filaments, which have a considerably smaller persistence length of 9–15 μm,[20,21] are unable to create membrane protrusions unless they are crosslinked into rigid bundles.[22] In narrow microchannels, the transverse thermal bending undulations of individual actin filaments can be confined, forcing the filaments to stretch,[23–25] similar to stretching of DNA chains in nanoslits.[26,27]

Aside from steric constraints provided by confinement, there are also packing constraints on filament organization coming from the fact that filaments cannot interpenetrate. The excluded volume of a pair of stiff filaments depends on their relative orientation: it is maximal when the filaments are perpendicular and minimal when the filaments are parallel. For filaments with only steric interactions, the lowest free energy state corresponds to a situation where the entropy is maximized. In dilute systems, the free volume will be large and the free energy is minimized by an isotropic distribution of rod orientations that maximizes the orientational entropy. At high densities, however, the reduced free volume will favor a transition to a nematic state with aligned rods. Rod alignment minimizes the excluded volume and thus maximizes the translational entropy, which offsets the loss in orientational entropy. For rigid rods, the isotropic to nematic (I–N) phase transition is governed by the aspect ratio of the rods, which is the ratio between their length, L, and diameter, D. According to the classic Onsager theory,[28] the transition occurs at a rod volume fraction $\phi = 3.340D/L$. Filament flexibility increases the threshold concentration at which the I–N transition occurs.[29–31] Solutions of actin filaments were shown[32,33] to undergo an I–N transition at a concentration of ~4 mg ml^{-1} (or $\phi = 0.4\%$), consistent with the Onsager prediction for filaments with a diameter of 7 nm and length in the range of ~10 to 20 μm. Moreover, reducing the filament length by capping with gelsolin shifted the I–N threshold to higher concentrations in inverse proportion to length.[34–37] It is uncertain whether the length and concentration of actin filaments *in vivo* favor a nematic state. The overall actin concentration in cells is typically at least 2 mg ml^{-1} and the filament length is around 1–2 μm.[38,39] However, both the concentration and the length depend on cell type and show spatiotemporal variations due to regulatory processes. In addition, a nematic transition may be counteracted by cross-linking proteins, some of which favor high angles between filaments.[40,41] Solutions of purified microtubules likewise undergo an I–N phase transition at concentrations consistent with the Onsager theory,[42] but *in vivo* microtubule organization is often dominated by nucleation and cross-linking effects.

We anticipate that confinement of cytoskeletal polymers at high density should generate a rich phase space, but so far there have been no experimental or theoretical studies in this regime. There have been studies of (nonbiological) rigid rods in quasi-2D confinement showing that interesting phase behavior emerges due to a competition between wall-induced rod alignment and bulk liquid crystalline ordering.[43,44] On a theoretical level, this behavior has only been studied by continuum theories[45] and simulations.[46] For semiflexible rods, such as actin filaments and microtubules, even more complex behavior is expected since the flexibility of the rods introduces enthalpic effects related to filament bending. So far, these enthalpic effects have only been studied for single chains[23,25] and in dilute systems with polymer volume fractions below the bulk I–N phase transition.[13–15] Theoretical models addressing geometrical confinement of semiflexible chains have also largely focused on single confined chains.[47–49] Therefore, the regime of dense confined polymers that is potentially relevant to cytoskeletal organization remains unexplored.

In this article, we study the combined effect of confinement and excluded volume interactions on the self-organization of actin filaments over a wide range of actin concentrations (0.1–7 mg ml^{-1}). To this end, we polymerize purified actin in microchambers produced by photolithography. Unlike intrinsically spherical liposomes or emulsion drops, these allow us to vary the geometrical shape and the degree of confinement in all three dimensions. We demonstrate that spatial confinement induces spontaneous bundling of the filaments above an actin concentration of 1 mg ml^{-1}, which is below the bulk I–N transition. We show that confinement-induced bundling requires that at least one confining dimension is comparable to the mean filament length. Finally, we propose a physical mechanism for bundling and discuss the potential physiological relevance of our findings.

Results

To study the effect of spatial confinement on filamentous (F-) actin self-organization, we fabricated cell-sized microchambers using photolithography. We could independently vary the degree of vertical confinement (by varying the chamber depth from 5 to 30 μm) and of lateral (in-plane) confinement. Moreover, we systematically varied the in-plane (lateral) shape and anisometry of the confining geometry. We prepared chambers with circular, square, triangular, and pill-shaped cross-sections. We could thus address the influence of wall curvature and chamber symmetry on actin organization. Moreover, the pill-shaped chambers mimic the shape of fission yeast cells,[4] while the polygonal shapes resemble shapes of mammalian cells on micropatterned adhesive islands[50–52] and in embryonic tissues.[8] The photoresist chip contained 1088 duplicate blocks, which each featured 19 chambers with different dimensions (Fig. 1A). This design enabled us to simultaneously observe networks under different confinement conditions and to test the reproducibility of actin organization. Typically 30% of the chambers were well-sealed, yielding around 300 testable/usable chambers of each size and shape. For all experimental conditions tested, actin networks in duplicate chambers had similar structures. Therefore, we could calculate ensemble-averaged quantities from image analysis. We typically analyzed images of 3–264 chambers per experimental condition. The chamber surfaces were passivated with κ-casein (bottom and side walls) and PEG-silane (top) to prevent actin adsorption (Fig. 1B). Actin was polymerized inside the chambers, in the presence of AlexaFluor488-phalloidin, which binds and stabilizes filamentous actin. Phalloidin raises the persistence length of actin filaments from 9 to 18 μm.[21] Moreover, the Alexa488 dye permitted visualization of F-actin by confocal laser scanning

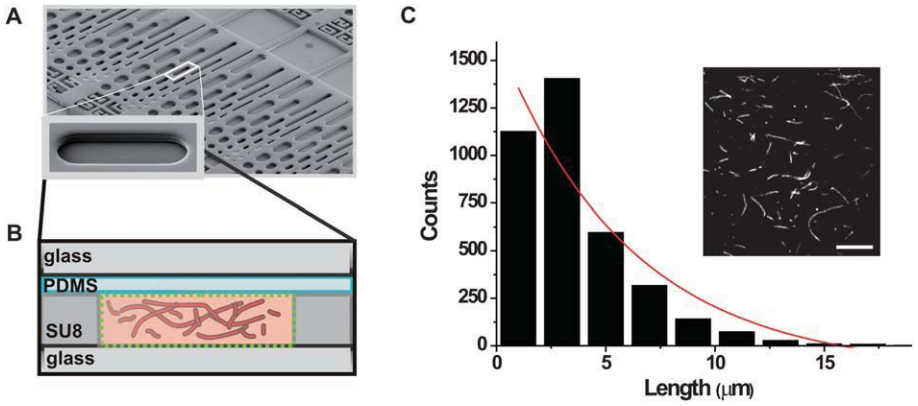

Fig. 1 Cell-sized confinement of actin networks in microfabricated chambers. (A) Scanning electron micrograph of a series of pill-shaped microchambers of varying size and aspect ratio. *Inset*: magnification of a 60 μm long chamber with an aspect ratio of 1 : 3. (B) Schematic side-view of an actin network confined in an SU8 photoresist chamber sealed with a PDMS-coated glass coverslip. All surfaces are coated with κ-casein (in green) to prevent nonspecific interactions with actin. The PDMS lid is additionally functionalized with PEG-silane. (C) Filament length distribution measured on 3711 actin filaments by fluorescence microscopy. The distribution is well-fit by an exponential (red line) giving an average filament length of 6 μm. Note that short filaments with lengths below 1 μm are underrepresented due to the diffraction-limited resolution of the optical microscope. *Inset*: typical confocal micrograph used for length distribution analysis, showing fluorescently labeled actin filaments embedded in an unlabeled network of 1 mg ml^{-1} actin. Around 0.3% of the filaments are labeled. Scale bar is 10 μm.

microscopy. The actin filaments had an exponential length distribution with a mean length of 6 μm (Fig. 1C). Networks were equilibrated for 6 hours after polymerization had been initiated. The networks looked similar when equilibrated for 24 hours.

We first observed the organization of actin networks in shallow (5 μm deep) chambers at different actin concentrations, ranging from 0.1 to 7 mg ml^{-1}. We tested three different confining geometries with circular, square and triangular cross-sections, keeping the in-plane (lateral) dimensions constant

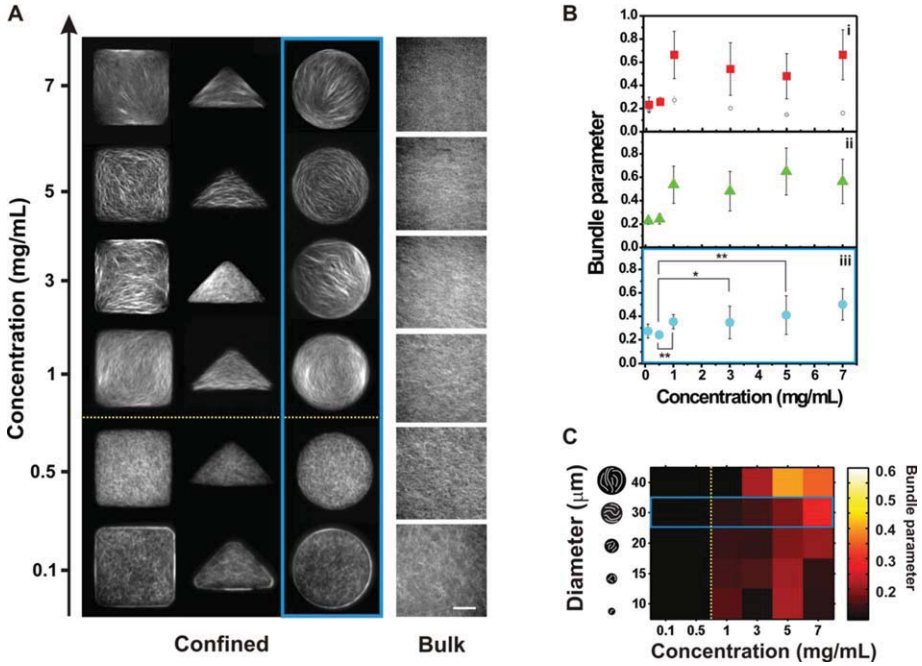

Fig. 2 Confined actin networks are homogeneous at low concentrations, but show filament alignment and bundling when the actin concentration exceeds 1 mg ml^{-1}. (A) *Left panel*: confocal micrographs of fluorescently labeled F-actin networks at different concentrations confined in chambers of different shapes but comparable size (circles of 30 μm diameter, squares and triangles with 30 μm sides). The chambers have a depth of 5 μm. *Right panel*: corresponding unconfined actin networks. Scale bar is 10 μM. (B) Bundle parameter *versus* actin concentration for chambers with cross-sections that are (i) square, (ii) triangular, and (iii) circular (~10–100 chambers per condition). Error bars represent S.D. of the mean. Asterisks denote statistically significant differences (* = $P < 0.05$, ** = $P < 0.001$). Grey open circles (in panel i) represent average bundle parameters of bulk actin networks. (C) Color map representation of the average bundle parameter in circular chambers as a function of chamber diameter and actin concentration (see side bar for color coding). Solid blue line demarcates *B*-values corresponding to (B)(iii), and vertical yellow dotted line divides the concentration axis into a homogeneous (left) and bundled (right) regime.

(30 μm). The two most dilute networks of 0.1 and 0.5 mg ml^{-1} were homogeneous and isotropic in all three types of chambers (Fig. 2A, *left panel*). However, at actin concentrations of 1 mg ml^{-1} and higher, the networks became inhomogeneous and partially aligned (images above the yellow dotted line). We observed dense, bundle-like structures, which aligned with the side walls in the chamber periphery and along the diagonal in the chamber center. In the remainder of the paper we will refer to these structures as "bundles", but we note that they have a different origin than conventional actin bundles formed in the presence of actin bundling agents.[40,41] The bundling was most clearly visible at 3 and 5 mg ml^{-1} actin. At 7 mg ml^{-1}, there was less image contrast between the bundles and the surrounding network.

We sought to quantify the bundling transition by image analysis, but this turned out to be challenging. It was impossible to identify and track the contours of individual actin filaments in the confocal images due to the small mesh size of the networks (300 nm at 1 mg ml^{-1}) and thermal fluctuations of the actin filaments. Identification of bundles by image thresholding was also impossible due to the low contrast between areas of low and high actin density (the typical ratio between pixel intensities of bundles *versus* background was only 1.5). For this reason, we decided to quantify the degree of bundling in each image with a *bundle parameter* based on a weighted average of the coherency of all pixels, where the weight was based on a thresholded image to select areas of high fluorescence intensity (see ESI†, Fig. S3). The coherency of a pixel is a dimensionless measure of the anisotropy of a small region around that pixel (ESI†, Fig. S2). The image analysis procedure is explained in detail in the ESI†. The bundle parameter can take values between 0, for networks that are homogeneous and isotropic, to 1, for bundles in a completely dark background. We obtained values ranging between 0.2, for homogeneous actin networks (reflecting density inhomogeneities and camera noise), and 0.7, for bundled actin networks (reflecting the non-zero intensity of the background), as illustrated in Fig. S3 (ESI†).

All the dilute (0.1 and 0.5 mg ml^{-1}) actin networks, which looked homogeneous by visual inspection, had a low bundle parameter of about 0.2 (solid symbols in Fig. 2Bi–iii). Dense networks (1–7 mg ml^{-1} actin) had a significantly larger bundle parameter of 0.5–0.65, in chambers with a square or triangular cross-section (Fig. 2Bi and ii, respectively). Dense networks in chambers with a circular cross-section also showed a statistically significant, though smaller, increase of the bundle parameter ~0.4 to 0.5 (Fig. 2Biii and S6†). The lateral chamber size did not change the concentration-dependence of the bundle parameter, as exemplified in Fig. 2C, for circular chambers ranging in diameter from 10 to 40 μm.

For comparison, we also examined bulk, unconfined samples at the same actin concentrations. In contrast to the confined networks, these samples remained homogeneous in density over the entire actin concentration range tested (Fig. 2A, *right panel*). The bundle parameter of the bulk networks was low (~0.2) and independent of the actin concentration (Fig. 2Bi, grey open circles). This finding implies that the aligned, bundle-like actin structures observed in microchambers are indeed caused by spatial confinement. Bulk actin networks are known to undergo an isotropic-to-nematic phase transition at a concentration that depends on the filament length.[32,35–37] In the fully labeled networks, we could not track individual actin filaments and their orientations. To circumvent this difficulty, we embedded trace amounts of fluorescent filaments in an otherwise dark actin background, labeling 1 out of every 500 filaments. As shown in Fig. S1A (ESI†), the tracer filaments are randomly oriented in bulk networks of 0.5–3 mg ml^{-1} actin, but they are aligned in bulk networks of 5–7 mg ml^{-1}. We quantified the degree of filament alignment by plotting histograms of the pixel orientations (ESI†, Fig S1B). The orientation angle for each pixel was determined from the local anisotropy of pixel intensities in a 5 × 5 pixel region centered on that pixel (ESI†). Below 5 mg ml^{-1}, the histograms show a broad distribution of angles, whereas at 5 and 7 mg ml^{-1}, the histograms develop a peak indicative of filament alignment. This indicates an isotropic to nematic transition at 5 mg ml^{-1}, consistent with prior experimental studies[32–37] and with the Onsager prediction for hard rods with a length of 6 μm.[28,29,31] Interestingly, the confinement-induced alignment of actin filaments started at an actin concentration of 1 mg ml^{-1} which is

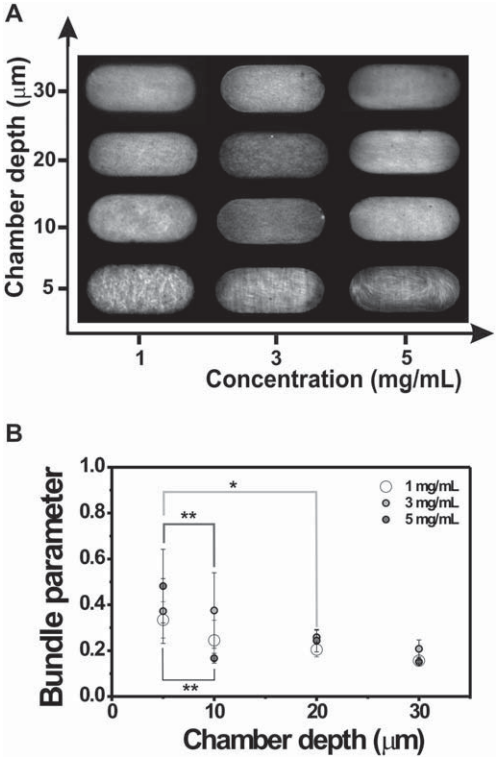

Fig. 3 Filament alignment and bundling in confined actin networks disappear when the depth of the microfabricated chambers is increased. (A) Confocal micrographs of fluorescently labeled F-actin networks at different actin concentrations in pill-shaped chambers of varying depths. The lateral dimensions are fixed to a minor diameter of 20 μm and major diameter of 40 μm. Filament bundling occurs only in 5 μm deep chambers, a depth similar to the average filament length. (B) Bundle parameter *versus* chamber depth for pill-shaped chambers, averaged over chambers with aspect ratios between 1 : 1 and 1 : 4 (fixed major diameter of 40 μm). Data are shown for actin concentrations of 1 mg ml^{-1} (white circles), 3 mg ml^{-1} (light gray circles) and 5 mg ml^{-1} (dark gray circles). Error bars represent S.D of the mean. Asterisks denote statistically significant differences (* = $P < 0.05$, ** = $P < 0.001$).

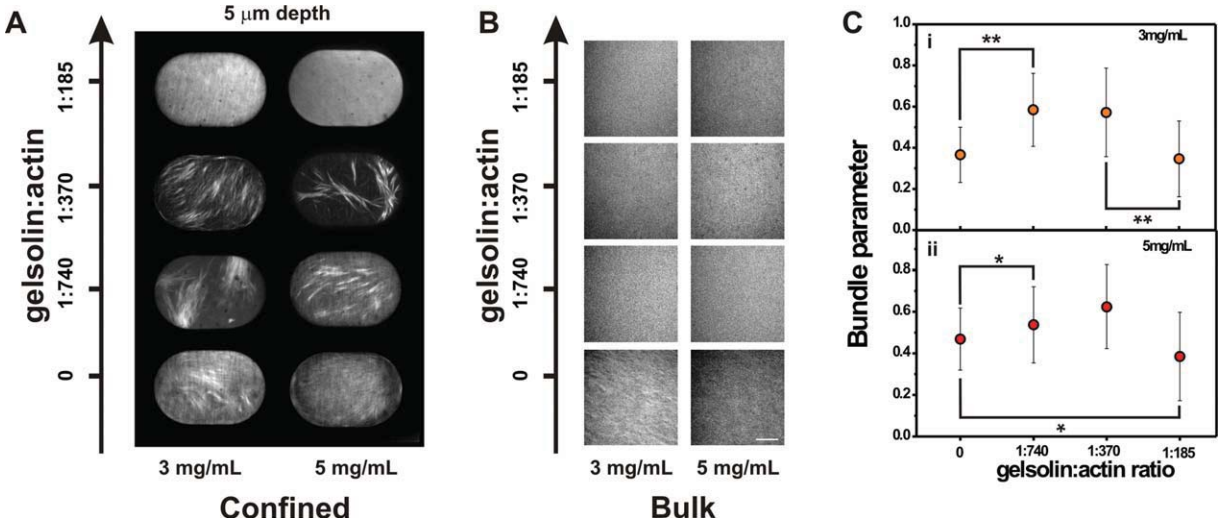

Fig. 4 Reducing the average filament length with the capping- and severing protein gelsolin enhances filament bundling up to a 1 : 370 gelsolin : actin ratio, while it homogenizes networks at a 1 : 185 ratio. (A) Confocal micrographs of F-actin networks in pill-shaped chambers (minor diameter 30 μm and major diameter 45 μm) at four different gelsolin : actin ratios, corresponding to estimated average lengths of 6, 2, 1 and 0.5 μm, for two different actin concentrations. (B) Control networks remain homogeneous at all gelsolin : actin ratios. Confocal micrographs of bulk F-actin networks with estimated average filament lengths of 6, 2, 1 and 0.5 μm, for two different actin concentrations. Scale bar is 10 μm. (C) Bundle parameter *versus* gelsolin : actin molar ratio in pill-shaped chambers, averaged over chambers with aspect ratios from 1 : 1 to 1 : 4 (fixed major diameter of 40 μm). Data are shown for actin concentrations of (i) 3 mg ml^{-1} and (ii) 5 mg ml^{-1}. Error bars represent S.D. of the mean. Asterisks represent statistically significant differences (* = $P < 0.05$, ** = $P < 0.001$).

substantially lower than the bulk phase transition point for liquid crystalline order.

The networks shown in Fig. 2A were confined in shallow chambers with depths of 5 μm. This depth is comparable to the average filament length, and 20% of the filaments even have a length that is larger than this depth. We therefore hypothesized that confinement-induced bundling in dense networks is caused by quasi-2D confinement, which tends to align the longest filaments in-plane. To test this hypothesis, we produced deeper chambers. Indeed, as soon as the chamber depth was increased from 5 μm to 10 μm or more, confinement-induced bundling disappeared, as illustrated by the confocal images in Fig. 3A of actin in pill-shaped chambers. The sudden disappearance of bundling was also reflected in significant jumps of the bundle parameter, from 0.3 to 0.2 for 1 mg ml^{-1} actin, and from 0.5 to 0.2 for 5 mg ml^{-1} actin (white and dark gray circles in Fig. 3B, respectively). When the chamber depth was further increased, there was a small, though statistically significant, further decrease of the bundle parameter (ESI†, Fig. S7). At 3 mg ml^{-1} actin, the bundle parameter started to decrease when the chamber depth was increased from 10 to 20 μm (light gray circles in Fig. 3B). The loss of bundles with increased chamber depth occurred irrespective of the lateral dimensions of the chambers and the in-plane aspect ratio (ESI†, Fig. S8). These findings suggest that confinement requires one of the chamber dimensions to be comparable to the mean filament length. Under these conditions, a substantial fraction of the filaments is confined to a quasi-2D microenvironment, since they cannot rotate out-of-plane.

As an independent test of the relation between confinement and filament length, we examined whether we could relieve confinement by decreasing the filament length while keeping a constant chamber depth of 5 μm. To control filament length we polymerized actin in the presence of the capping protein gelsolin, which caps filaments at the barbed (fast-growing) ends.[53] The mean filament length L decreases with increasing gelsolin : actin molar ratio, R_{GA}, as $L = (1/370\ R_{GA})$.[53] Remarkably, addition of 1 : 740 or 1 : 370 gelsolin to actin networks of 3 and 5 mg ml^{-1} caused the formation of distinct bundles which appeared thicker than in networks made in the absence of gelsolin (Fig. 4A), even though the average filament length was less than the chamber depth (2 and 1 μm, respectively). The ratio of pixel intensities between bundles and background was 2–3, which was higher than in networks without gelsolin (where the ratio was ~1.5). When the gelsolin level was further increased to 1 : 185, corresponding to a mean filament length of 0.5 μm (10-fold less than the chamber depth), the networks did become homogeneous (Fig. 4A). In contrast, control bulk networks remained homogeneous irrespective of actin concentration and gelsolin : actin ratio (Fig. 4B). The bundle parameter confirmed the trends seen by visual inspection, increasing from ~0.4 to ~0.6 upon addition of 1 : 740 gelsolin, and going back down to ~0.4 with 1 : 185 gelsolin, both at 3 mg ml^{-1} and 5 mg ml^{-1} actin (Fig. 4C). The increased bundle parameter of networks with 1 : 740 or 1 : 370 gelsolin compared to networks without gelsolin was statistically significant at both 3 and 5 mg ml^{-1} actin, but the decreased bundle parameter at 1 : 185 gelsolin was only significant at 5 mg ml^{-1} (ESI†, Fig. S9). The gelsolin-dependent bundling was independent of the lateral dimensions and in-plane anisometry of pill-shaped chambers, though the gelsolin concentration where the bundle parameter reached a maximum was either 1 : 370 or 1 : 740 depending on actin concentration and chamber anisometry (ESI†, Fig. S10).

The orientation of the actin bundles is expected to reflect a competition between alignment effects near the walls and

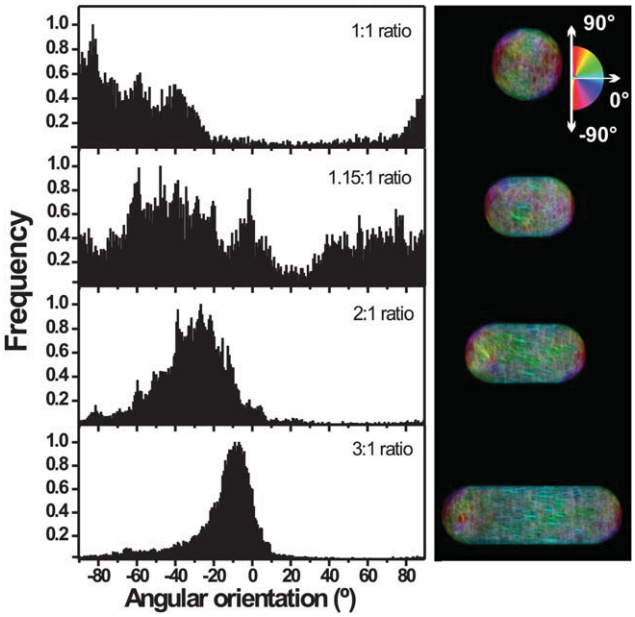

Fig. 5 Actin bundle-like structures reorient along the long axis of pill-shaped chambers when the chambers become more anisotropic. *Left panel*: histograms of pixel orientation angles for different chamber aspect ratios for networks of 7 mg ml^{-1} actin; the minor axis of all chambers is 20 μm. The histograms were calculated for the (single) images shown on the right. *Right panel*: color map of the orientation angles superposed on raw fluorescence intensity data. The semicircle color scale represents orientation angles in degrees.

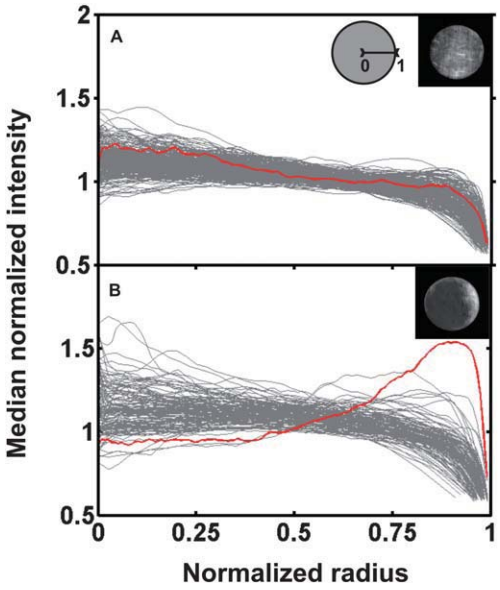

Fig. 6 There is no peripheral accumulation of actin in circular chambers. The radially averaged fluorescence intensity normalized by the median intensity and by perimeter length is shown as a function of radial distance from the chamber center. The distance is normalized by the chamber radius, so a value of 1 corresponds to the edge and 0 corresponds to the center. Each gray trace represents one individual chamber. (A) For $N = 264$ chambers containing 3 mg ml^{-1} actin there is no obvious actin accumulation at the chamber edge. The intensity dip corresponds to the abrupt passage from the inside of a bright chamber to the dark background with zero intensity outside. Red trace corresponds to example chamber in the inset. (B) For $N = 126$ chambers containing 3 mg ml^{-1} actin and gelsolin (1 : 740 gelsolin : actin) there is also no obvious actin accumulation at the chamber edge, except for one example (red trace and the inset).

packing constraints in the center. We tested whether we could influence the direction of bundle alignment by elongating the chambers in one direction. We compared actin networks of 3 mg ml^{-1} in the presence of 1 : 740 gelsolin confined in shallow, pill-shaped chambers with length over width ratios going from 1 (circular) to 3 : 1. Fig. 5 (*left panel*) shows histograms of the orientation angles of pixel anisotropies calculated for the images shown on the right. The distribution of orientation angles shifts from being wide and multipeaked at chamber aspect ratios of 1 and 1.5 : 1 to a more narrow distribution peaking close to an angle of zero degrees with the long axis for aspect ratios of 2 and 3. This indicates progressive alignment of the bundles along the long axis of the chambers, which can also be seen when an orientation color map is overlaid on the original fluorescence micrographs (Fig. 5, *right panel*). This alignment with the long axis is reminiscent of patterns reported for microtubules in rectangular microchambers.[18]

For semiflexible polymers, confinement influences not only the configurational entropy, but also the elastic energy associated with polymer bending. Theoretical models predict that long polymers will accumulate at the confining boundary to minimize their curvature and the associated energy cost.[54,55] This prediction was confirmed for actin networks in spherical geometries (liposomes and emulsions droplets)[14,15] and for microtubules in emulsion droplets[19] and rectangular chambers.[13] Confocal images of confined actin networks in microchambers did not indicate preferential accumulation of actin at the periphery (see for example Fig. 2A and 4A). To quantify the dependence of actin density on the radial distance from the chamber center, we calculated the radially averaged pixel intensity (normalized by perimeter) as a function of the radial distance from the chamber edge to the center (as explained in the ESI†). We focused on 3 mg ml^{-1} actin networks in pill-shaped chambers of various sizes (minor axis 10–40 μm) and aspect ratios (1 : 1 to 1 : 4). In the absence of gelsolin, the radially averaged pixel intensity normalized by the median intensity remained constant and close to 1 from the edge till the center (Fig. 6A, 264 chambers were analyzed; each trace represents one chamber), corresponding with the visual observation that the confocal images showed no clear radial dependence (red trace and the inset of Fig. 6A). The apparent drop in intensity at the edge originates from the abrupt transition from the bright chamber edge to the dark exterior. In the presence of gelsolin, there was similarly no evidence of actin accumulation at the chamber edge (Fig. 6B). Out of a total of 126 chambers, we observed only one chamber with edge accumulation (red trace and the inset). These results demonstrate that there is no preferential accumulation of actin at the periphery.

Discussion

By fluorescence imaging of actin networks in microchambers, we discovered that cell-sized confinement can induce spontaneous formation of dense bundle-like structures. This filament bundling required actin concentrations of at least 1 mg ml^{-1}, implying

a collective phenomenon dependent on filament–filament interactions. The onset concentration for confinement-induced bundling is substantially lower than the I–N phase transition of corresponding unconfined actin solutions, which occurred at 5 mg ml^{-1}. The in-plane dimensions (over a range of 10 to 200 μm) and shape of the chambers had no influence on the extent of filament bundling or on its dependence on actin concentration. However, the geometry of the confining boundaries did affect the orientation of the actin bundles. Bundles had a tendency to orient mainly along the diagonal in the center of the chambers and along the walls in the periphery. In pill-shaped chambers with a length/width ratio above 2, bundles oriented along the long axis.

While the lateral dimensions had no influence on filament bundling, the vertical depth of the chambers was a crucial factor. Filament bundling required shallow chambers with a depth of 5 μm, similar to the average filament length. Chambers with depths of 10 μm or more did not induce filament bundling (at least not for the actin concentrations explored of up to 5 mg ml^{-1}). This observation suggests that physically induced actin bundling requires quasi-2D confinement. The actin filaments have a highly polydisperse length distribution, ranging from below 1 μm to 18 μm. A sizeable fraction (20%) of the filaments is longer than 5 μm and therefore forced to remain in-plane in the shallow chambers. Increasing the chamber depth relieves this in-plane confinement (sketched in Fig. 7A).

Theory and simulations predict that confinement of rods between parallel surfaces encourages rod alignment,[55,56] and indeed such alignment was shown for microtubules in thin planar slits.[55] However, for polymers interacting by steric interactions only, we would, at first glance, not expect any density inhomogeneities or bundling. However, the actin filaments have a highly polydisperse length distribution, and 80% of the filaments are shorter than the chamber depth and can freely rotate out-of-plane. It is conceivable that these short filaments cause an attractive interaction between the long filaments purely due to steric interactions. Such an entropic depletion effect is well-established for bidisperse suspensions of short and long rods.[57–59] When two long rods aligned in parallel come closer than a distance equal to the width of a short rod, the short rods are excluded from the overlap zone (Fig. 7B). This results in a higher osmotic pressure outside the long rods than in between them, driving them together. The short actin filaments may therefore promote bundling of the longer filaments. When two aligned long rods come closer than a distance equal to the length of a short rod, the short rods are forced to align, which would also lead to an entropic cost. Intriguingly, recent experiments on systems of vibrofluidized rigid rods in the presence of spheres, mimicking depletion agents, have shown that this type of bundling can indeed occur, an effect also corroborated by equilibrium Monte Carlo simulations.[60] Although the system studied there is purely 2D, and only bidisperse, with rod aspect ratios far

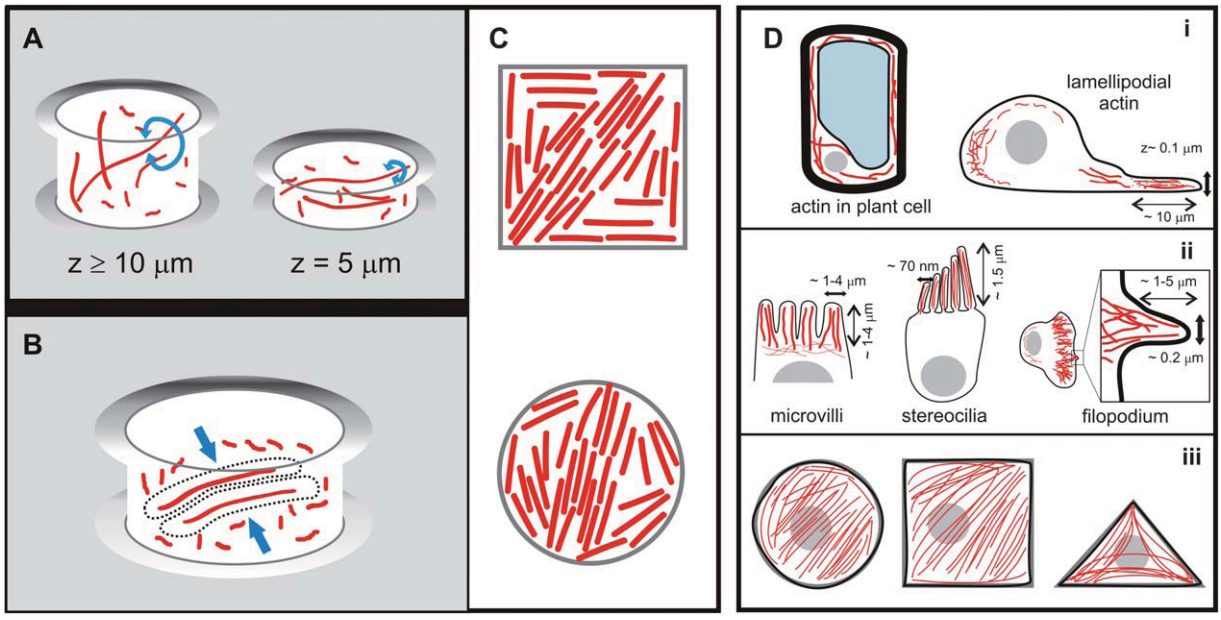

Fig. 7 Possible mechanisms for spontaneous filament alignment and bundling in confined actin networks, and possible implications for the *in vivo* cytoskeleton. (A) Chambers with a depth that exceeds the length of the filaments do not impose confinement, because the filaments can freely rotate and explore all three dimensions (aside from chain entanglements). Shallow chambers with a depth less than the average filament length provide quasi-2D confinement, since a large fraction of the filaments cannot freely rotate and is therefore effectively confined in-plane. (B) A polydisperse length distribution may cause filament bundling due to an entropic depletion effect, where short filaments generate an attractive depletion interaction between the longer ones (blue arrows). (C) The organization of hard rod liquid crystals in quasi-2D confinement is determined by a competition between rod alignment along the walls and rod nematization in the chamber center. For rods in square or circular wells this competition creates topological defects at opposite poles. (D) Examples of *in vivo* situations where actin filaments are confined. (i) Quasi-2D environment of actin networks in the thin cytoplasmic region between the cell wall and vacuole of plant cells and in the thin lamellipodium of migrating animal cells. (ii) Quasi-1D confinement of actin filaments in membrane protrusions. (iii) Quasi-2D confinement *in vivo* can be artificially generated by spatially confining cells to micropatterned adhesive islands of defined geometry.

smaller than in the actin system, those findings show that depletion effects can be expected to have a major impact on the spatial organization of rod systems in a quasi 2D geometry. The presence of a depletion effect may explain the counterintuitive observation that filaments shortened with gelsolin showed more pronounced bundling than unshortened filaments. Shortening should relieve in-plane confinement of the filaments, but the length distribution is still polydisperse so there may still be depletion-induced bundling. Furthermore, there can be a feedback effect since bundles formed in the absence of proteins that regulate bundle length tend to be longer than individual filaments and therefore do experience *z*-confinement. Bundling may also occur more readily at shorter overall filament length, because kinetic constraints on filament motion originating from chain entanglements are reduced.[32] Reducing the average length to 0.5 μm (1 : 185 gelsolin) did lead to bundle disappearance, as expected, since the average length was tenfold less than the chamber depth. An additional contributing factor to the loss of bundles could be a smaller size mismatch between the shortest and longest filaments in the presence of high gelsolin concentrations.

We could not find any evidence for peripheral accumulation of actin in the microfabricated chambers, in contrast to prior studies of actin networks in liposomes or emulsion drops which formed thin cortical shells.[14,15] Similar observations of peripheral accumulation exist for microtubules in emulsion drops and microchambers[13,19] and for DNA in viral capsids.[48] Semiflexible polymers can remain homogeneously distributed inside a sphere volume when short, but long filaments are forced to bend. The energy cost associated with this bending is minimized when the filaments accumulate at the sphere surface.[13] It is possible that the actin filaments studied here were too short for the bending enthalpy to be relevant. It is also possible that excluded volume interactions between filaments present at the high densities studied here introduce energy terms that compete with the single-polymer effect of bending enthalpy. Bending enthalpy may still play a role in controlling the alignment of actin bundles. Alignment of peripheral bundles along the walls and alignment of central bundles along the long axis in elongated chambers are certainly consistent with a minimization of the bending energy.

The actin patterns in the microfabricated chambers are strikingly similar to patterns recently observed for vibrofluidized granular rods confined in flat chambers with circular or square cross-sections.[43,44] Similar to the actin filament bundles in microchambers with circular and square cross-sections (Fig. 2A), granular rods close to the walls aligned parallel with the wall, while rods in the center aligned with each other, straight across the chamber. Competition between alignment of rods in the bulk and near the boundaries produced patterns with topological defects (sketched in Fig. 7C). These patterns were interpreted in terms of a continuum theory for liquid crystals accounting for wall-anchoring and elastic distortions of the bulk nematic phase.[61,62] The similarity of the granular rod structures to the actin structures and the dominance of excluded volume interactions in both systems suggest that a similar liquid crystal theory may perhaps be formulated for the confined actin system. However, it is presently unclear how to account for microscopic properties such as the finite size of the filaments, the polydisperse length distribution which introduces depletion effects, and the flexibility of the filaments, which introduces bending enthalpy contributions.

We showed that nonadhesive hard-wall boundaries can cause the formation of bundle-like actin structures whose alignment depends on the shape and anisometry of the confinement. Intracellular organization of actin often occurs in highly confined compartments. Animal cells migrating on rigid adhesive surfaces for instance extend a flat lamellipodium which is nearly 2D with a thickness of only ~0.1 to 0.2 μm[9–11] (Fig. 7Di). Plant cells have a very thin cytoplasmic layer of only ~1 μm containing actin filaments with a definite orientation which facilitates cytoplasmic streaming.[63] Animal cells also extend different types of finger-like membrane protrusions filled with actins such as filopodia and stereocilia, which have a thickness of less than 100 nm[12,64] (Fig. 7Dii). However, contrary to filaments in microfabricated chambers, F-actin is not only confined passively. In addition to the effect of cellular boundaries there are the effects of a variety of actin-binding proteins that facilitate the formation of dendritic networks in the lamellipodium and rigid bundles that deform the plasma membrane.[65] Bundles of actin filaments and myosin motors, known as stress fibers, actively create contractile tension, which promotes spreading of cells on rigid adhesive substrates into flat, quasi-2D shapes. Nevertheless, it is possible that the confined geometries created by actin filaments feed back on the organization of the actin filaments. For instance, spontaneous alignment and densification of actin filaments induced by confinement in tube-like membrane protrusions may promote F-actin bundling by actin-binding proteins.[66] Indeed, some actin-binding proteins have been shown to form bundles of actin filaments only when these filaments are aligned nearly parallel.[67] However, confinement effects by themselves cannot explain the unipolar direction of actin filaments in many *in vivo* bundles, which likely requires regulated nucleation of actin filament growth and a polarity preference of certain actin-bundling proteins.[67,68]

A natural follow-up to our work would be to functionalize the walls of the microchambers with proteins that couple actin filaments to the cell boundaries or which nucleate actin filament growth.[2] There is already evidence from studies with flat substrates patterned with islands of actin-nucleating proteins of varying geometries, that spatial patterning of actin nucleation has profound effects on actin self-organization.[69] It would also be very interesting to encapsulate contractile actin–myosin cables into microfabricated chambers with adhesive walls, since this could help to mimic the effect of cell shape on the organization of actin stress fibers seen in cells cultured on μm sized extracellular matrix islands of defined geometry created using microfabrication techniques[50–52] (Fig. 7Diii).

Conclusions

In this paper we studied the effect of spatial confinement on self-organization of actin by polymerizing actin inside cell-sized microchambers made by photolithography. We found that confinement induces spontaneous formation of bundle-like structures. We showed that this spontaneous alignment only occurs above a threshold actin concentration of 1 mg ml^{-1}, indicating a collective phenomenon that relies on excluded volume interactions between the filaments. Furthermore,

alignment occurred only in shallow chambers, implying that quasi-2D confinement is important. The lateral dimensions of the chambers did not influence the ordering transition. The shape of the chambers influenced the orientation of the bundles. Bundles in circular and square chambers aligned along the wall and along the chamber diagonal. Bundles in pill-shaped chambers with length/width ratios of 2 or more predominantly oriented along the long axis. We propose that confinement-induced actin bundling is driven by steric repulsions of the filaments with each other and the walls. The quasi-2D confinement aligns the longest actin filaments in-plane, and the shortest actin filaments may push the longer ones into dense bundles by an entropic depletion effect. Minimization of the bending energy of the semiflexible filaments may contribute to the alignment of bundles along the chamber periphery and diagonal/long axis. This physical mechanism may influence intracellular organization of actin in conjunction with biochemical regulation and actin/membrane adhesion.

Materials and methods

Materials

Monomeric G-actin was purified from rabbit psoas skeletal muscle without column purification.[70] G-actin was stored at −80 °C in G-buffer (2 mM Tris–HCl, 0.2 mM Na_2ATP, 0.2 mM $CaCl_2$, 0.2 mM dithiothreitol (DTT), 0.5 mM NaN_3, pH 8.0). The actin concentration was determined by absorbance measurements at 290 nm using an extinction coefficient of 1.1 $cm^2\ mg^{-1}$.[65] Recombinant human plasma gelsolin purified from *Escherichia coli* was a kind gift from Fumihiko Nakamura (Harvard Medical School, Boston). We resuspended gelsolin in G-buffer at a concentration of 1 μM. ATP was prepared as a 100 mM MgATP stock solution using equimolar amounts of Na_2ATP and $MgCl_2$ in a 10 mM imidazole–HCl buffer (pH 7.4). Rhodamine-phalloidin was from Sigma Aldrich and Alexa 488-phalloidin was from Molecular Probes (Invitrogen). Other chemicals were purchased from Sigma Aldrich.

Confinement assays

We prepared G-actin solutions on ice, in assembly buffer with final concentrations of 25 mM imidazole–HCl, 50 mM KCl, 0.1 mM MgATP, 2 mM $MgCl_2$, 1 mM DTT, and pH 7.4. We stabilized the actin filaments with an equimolar amount of fluorescent Alexa 488-phalloidin. The buffer contained 2 mM trolox to minimize photobleaching. The G-actin concentration was varied between 0.1 and 7 mg ml^{-1} (1 mg ml^{-1} corresponds to a molar concentration of 23.8 μM). To determine the filament length distribution, a low density of pre-polymerized filaments was embedded in unlabeled networks of 1 mg ml^{-1} actin. The lengths were measured for 3711 filaments from confocal micrographs using the NeuronJ plugin of ImageJ (http://rsbweb.nih.gov/ij/). To alter the length distribution, gelsolin was included in the mixture at different molar ratios to G-actin. G-actin was always added last, to prevent premature actin polymerization, and 25 μL of the solution was immediately pipetted onto a chip with microchambers and the chambers were sealed with a polydimethylsiloxane (PDMS)-coated glass microscope slide. Actin polymerization was initiated by warming the samples to room temperature. The SU8 and glass surfaces of the chambers were passivated beforehand with 0.1 mg ml^{-1} κ-casein, and the PDSM lid was passivated with PEG-silane (2-[methoxy(polyethyleneoxy)propyl]trimethoxysilane, ABCR). Microchamber lithography procedures, surface treatments and lid preparation are described in detail in the Materials and methods section of the ESI†.

Bulk assays

To test whether actin filament alignment in chambers was caused by confinement, we prepared control, unconfined actin samples in large chambers consisting of a glass slide and coverslip separated by 25 μm thick spacers of Fluorinated Ethylene Propylene Copolymer (GoodFellow). Surfaces were passivated in the same way as microchambers with 0.1 mg ml^{-1} κ-casein prior to sample inclusion. The spacers were lined with vacuum grease along the inner sides to prevent sample leakage and the chambers were sealed with vacuum grease to prevent solvent evaporation.

Fluorescence microscopy

Samples were observed with a spinning disk confocal scanner (CSU22, Yokogawa Electric Corp.) on a DMIRB Leica inverted microscope. The AlexaFluor488-dye was excited with 488 nm laser light (Coherent Inc.) and images were recorded with a cooled EM-CCD camera (C9100, Hamamatsu Photonics) using an exposure time of 50–100 ms. Image stacks were obtained by scanning through the z-direction in steps of 100 nm with a piezo-driven 100× (1.3 NA) oil immersion objective (PL Fluotar Leica).

Statistics

Data are shown as averages ± S.D. Means were compared using unpaired Student's t-tests.

Acknowledgements

This work is part of the research program of the Foundation for Fundamental Research on Matter, which is financially supported by the Netherlands Organisation for Scientific Research (NWO). This work was funded by a VIDI grant from NWO (JA and GK). We thank C. Rétif and G. Vollenbroek for help with microfabrication, and R. Dries, I. Garlea, and D. Sage (EPFL) for helpful discussions.

References

1 C. Revenu, R. Athman, S. Robine and D. Louvard, The co-workers of actin filaments: from cell structures to signals, *Nat. Rev. Mol. Cell Biol.*, 2004, **5**, 635–646.
2 M. P. Sheetz, J. E. Sable and H.-G. Döbereiner, Continuous membrane-cytoskeleton adhesion requires continuous accomodation to lipid and cytoskeleton dynamics, *Annu. Rev. Biophys. Biomol. Struct.*, 2006, **35**, 417–434.
3 F. Julicher, A. Adjari and J. Prost, Modeling molecular motors, *Rev. Mod. Phys.*, 1997, **69**, 1269–1282.
4 B. Alberts, A. Johnson, J. Lewis, M. Raff, K. Roberts and P. Walter, *Molecular Biology of the Cell*, Garland Science, New York, 2008.
5 B. Gunning and M. Steer, *Plant Cell Biology, Structure and Function*, Jones & Bartlett Learning, Boston, 1996.

6 M. Tanaka, M. Tutus, S. Kaufmann, F. Rossetti, E. Schneck and I. Weiss, Wetting and dewetting of extracellular matrix and glycocalix models, *J. Phys.: Condens. Matter*, 2005, **17**, 649–663.
7 N. Nijenhuis, D. Mizuno, J. Spaan and C. Schmidt, Viscoelastic response of a model endothelial glycocalyx, *Phys. Biol.*, 2009, **6**, 025014–025022.
8 R. Fernandez-Gonzalez, S. de M. Simoes, J.-C. Röper, S. Eaton and J. A. Zallen, Myosin II dynamics are regulated by tension in intercalating cells, *Dev. Cell*, 2009, **17**, 736–743.
9 J. V. Small, M. Herzog and K. Anderson, Actin filament organization in the fish keratocyte lamellipodium, *J. Cell Biol.*, 1995, **129**, 1275–1286.
10 A. Verkhovsky, O. Chaga, S. Schaub, T. Svitkina, J. Meister and G. Borisy, Orientational order of the lamellipodial actin network as demonstrated in living motile cells, *Mol. Biol. Cell*, 2003, **14**, 4667–4675.
11 E. Urban, S. Jacob, M. Nemethova, G. P. Resch and J. V. Small, Electron tomography reveals unbranched networks of actin filaments in lamellipodia, *Nat. Cell Biol.*, 2010, **12**, 429–435.
12 E. S. Chhabra and H. N. Higgs, The many faces of actin: matching assembly factors with cellular structures, *Nat. Cell Biol.*, 2007, **9**, 1110–1121.
13 M. Lagomarsino, C. Tanase, J. Vos, A. Emons, B. Mulder and D. Marileen, Microtubule organization in three-dimensional confined geometries: evaluating the role of elasticity through a combined in vitro and modeling approach, *Biophys. J.*, 2007, **92**, 1046–1057.
14 M. M. A. E. Claessens, R. Tharmann, K. Kroy and A. R. Bausch, Microstructure and viscoelasticity of confined semiflexible polymer networks, *Nat. Phys.*, 2006, **2**, 186–189.
15 L. Limozin, M. Bärmann and E. Sackmann, On the organization of self-assembled actin networks in giant vesicles, *Eur. Phys. J. E: Soft Matter Biol. Phys.*, 2003, **10**, 319–330.
16 M. Elbaum, D. Fygenson and A. Libchaber, Buckling microtubules in vesicles, *Phys. Rev. Lett.*, 1996, **76**, 4078–4081.
17 V. Emsellem, O. Cardoso and P. Tabeling, Vesicle deformation by microtubules: a phase diagram, *Phys. Rev. E: Stat. Phys., Plasmas, Fluids, Relat. Interdiscip. Top.*, 1998, **58**, 4807–4810.
18 S. Cortes, N. Glade, I. Chartier and J. Tabony, Microtubule self-organisation by reaction-diffusion processes in miniature cell-sized containers and phospholipid vesicles, *Biophys. Chem.*, 2006, **120**, 168–177.
19 M. Pinot, F. Chesnel, J. Kubiak, I. Arnal, F. Nedelec and Z. Gueroui, Effects of confinement on the self-organization of microtubules and motors, *Curr. Biol.*, 2009, **19**, 954–960.
20 F. Gittes, B. Mickey, J. Nettleton and J. Howard, Flexural rigidity of microtubules and actin filaments measured from thermal fluctuations in shape, *J. Cell Biol.*, 1993, **120**, 923–934.
21 H. Isambert, P. Venier, A. Maggs, A. Fattoum, R. Kassab, D. Pantaloni and M. Carlier, Flexibility of actin filaments derived from thermal fluctuations. Effect of bound nucleotide, phalloidin, and muscle regulatory proteins, *J. Biol. Chem.*, 1995, **270**, 11437–11444.
22 M. Honda, K. Takiguchi, S. Ishikawa and H. Hotani, Morphogenesis of liposomes encapsulating actin depends on the type of actin-crosslinking, *J. Mol. Biol.*, 1999, **287**, 293–300.
23 S. Köster, D. Steinhauser and T. Pfhol, Brownian motion of actin filaments in confining microchannels, *J. Phys.: Condens. Matter*, 2005, **17**, S4091.
24 M. Choi, C. Santangelo, O. Pelletier, J. Kim, S. Kwon, Z. Wen, Y. Li, P. Pincus, C. Safinya and M. Kim, Direct observation of biaxial confinement of a semiflexible filament in a channel, *Macromolecules*, 2005, **38**, 9882–9884.
25 L. Hirst, E. Parker, Z. Abu-Samah, Y. Li, R. Pynn, N. MacDonald and C. Safinya, Microchannel systems in titanium and silicon for structural and mechanical studies of aligned protein self-assemblies, *Langmuir*, 2005, **21**, 3910–3914.
26 J. Tegenfeldt, C. Prinz, H. Cao, S. Chou, W. Reisner, R. Riehn, Y. Wang, E. Cox, J. Sturm, P. Silberzan and R. Austin, The dynamics of genomic-length DNA molecules in 100 nm channels, *Proc. Natl. Acad. Sci. U. S. A.*, 2004, **101**, 10979–10983.
27 D. Bonthuis, C. Meyer and C. Dekker, Conformation and dynamics of DNA confined in slit-like nanofluidic channels, *Phys. Rev. Lett.*, 2008, **101**, 108303–108304.
28 L. Onsager, The effects of shape on the interaction of colloidal particles, *Ann. N. Y. Acad. Sci.*, 1949, **51**, 627–659.
29 A. Khokhlov and A. Semenov, Liquid-crystalline ordering in the solution of partially flexible macromolecules, *Phys. A*, 1982, **112**, 605–614.
30 Z. Y. Chen, Nematic ordering in semiflexible polymer chains, *Macromolecules*, 1993, **26**, 3419–3423.
31 T. Odijk, Theory of lyotropic polymer liquid crystals, *Macromolecules*, 1986, **19**, 2313–2329.
32 J. Kaes, H. Strey, J. Tang, D. Finger, R. Ezzell, E. Sackmann and P. Janmey, F-actin, a model polymer for semiflexible chains in dilute, semidilute, and liquid crystalline solutions, *Biophys. J.*, 1996, **70**, 609–625.
33 E. Helfer, P. Panine, M. Carlier and P. Davidson, The interplay between viscoelastic and thermodynamic properties determines the birefringence of F-actin gels, *Biophys. J.*, 2005, **89**, 543–553.
34 A. Suzuki, T. Maeda and T. Ito, Formation of liquid crystalline phase of actin filament solutions and its dependence on filament length as studied by optical birefringence, *Biophys. J.*, 1991, **59**, 25–30.
35 R. Furukawa, R. Kundra and M. Fechheimer, Formation of liquid crystals from actin filaments, *Biochemistry*, 1993, **32**, 12346–12352.
36 C. Coppin and P. Leavis, Quantitation of liquid-crystalline ordering in F-actin solutions, *Biophys. J.*, 1992, **63**, 794–807.
37 J. Viamontes, P. Oakes and J. X. Tang, Isotropic to nematic liquid crystalline phase transition of F-actin varies from continuous to first order, *Phys. Rev. Lett.*, 2006, **97**, 118103–118107.
38 J. Podolski and T. Steck, Length distribution of F-actin in Dictyostelium discoideum, *J. Biol. Chem.*, 1990, **265**, 1312–1318.
39 T. Svitkina, A. Verkhovsky, K. McQuade and G. Borisy, Analysis of the actin-myosin II system in fish epidermal keratocytes: mechanism of cell body translocation, *J. Cell Biol.*, 1997, **139**, 397–415.
40 C. Thomas, S. Tholl, D. Moes, M. Dieterle, J. Papuga, F. Moreau and A. Steinmetz, Actin bundling in plants, *Cell Motil. Cytoskeleton*, 2009, **66**, 940–957.
41 Y. Puius, N. Mahoney and S. Almo, The modular structure of actin-regulatory proteins, *Curr. Opin. Cell Biol.*, 1998, **10**, 23–34.
42 A. Hitt, A. Cross and R. Williams, Microtubule solutions display nematic liquid crystalline structure, *J. Biol. Chem.*, 1990, **265**, 1639–1647.
43 J. Galanis, D. Harries, D. Sackett, W. Losert and R. Nossal, Spontaneous patterning of confined granular rods, *Phys. Rev. Lett.*, 2006, **96**, 028002–028006.
44 J. Galanis, R. Nossal, W. Losert and D. Harries, Nematic order in small systems: measuring the elastic and wall-anchoring constants in vibrofluidized granular rods, *Phys. Rev. Lett.*, 2010, **105**, 168001–168005.
45 E. Gartland, P. Palffy-Muhoray and R. Varga, Numerical minimization of the Landau-de Gennes free energy: defects in cylindrical capillaries, *Mol. Cryst. Liq. Cryst.*, 1991, **199**, 429–452.
46 Y. Trukhina and T. Schilling, Computer simulation study of a liquid crystal confined to a spherical cavity, *Phys. Rev. E: Stat., Nonlinear, Soft Matter Phys.*, 2008, **77**, 011701(7).
47 F. Wagner, G. Lattanzi and E. Frey, Conformations of confined biopolymers, *Phys. Rev. E: Stat., Nonlinear, Soft Matter Phys.*, 2007, **75**, 050902(4).
48 F. Nedelec and D. Foethke, Collective Langevin dynamics of flexible cytoskeletal fibers, *New J. Phys.*, 2007, **9**, 1367–2630.
49 N. Oskolkov, P. Linse, I. Potemkin and A. Khokhlov, Nematic ordering of polymers in confined geometry applied to DNA packaging in viral capsids, *J. Phys. Chem. B*, 2011, **115**, 422–432.
50 R. Singhvi, A. Kumar, G. Lopez, G. Stephanopoulos, D. Wang, G. Whitesides and D. Ingber, Engineering cell shape and function, *Science*, 1994, **264**, 696–698.
51 M. Théry, V. Racine, M. Piel, A. Pépin, A. Dimitrov, Y. Chen, J. Sibarita and M. Bornens, Anisotropy of cell adhesive microenvironment governs cell internal organization and orientation of polarity, *Proc. Natl. Acad. Sci. U. S. A.*, 2006, **103**, 19771–19776.
52 C. Chen, M. Mrksich, S. Huang, G. Whitesides and D. Ingber, Geometric control of cell life and death, *Science*, 1997, **276**, 1425–1428.
53 S. Burlacu, P. A. Janmey and J. Borejdo, Distribution of actin filament lengths measured by fluorescence microscopy, *Am. J. Physiol. Cell Physiol.*, 1992, **262**, C569–C577.
54 Y. Liu and B. Chakraborty, Shapes of semiflexible polymers in confined spaces, *Phys. Biol.*, 2008, **5**, 026004–026012.
55 M. Lagomarsino, M. Dogterom and M. Dijkstra, Isotropic-nematic transition of long, thin, hard spherocylinders confined in a

quasi-two-dimensional planar geometry, *J. Chem. Phys.*, 2003, **119**, 3535–3540.
56 R. van Roij, M. Dijkstra and R. Evans, Orientational wetting and capillary nematization of hard-rod fluids, *Europhys. Lett.*, 2000, **49**, 350.
57 H. Lekkerkerker, P. Coulon, R. Haegen and R. Deblieck, On the isotropic-liquid crystal phase separation in a solution of rodlike particles of different lengths, *J. Chem. Phys.*, 1984, **80**, 3427–3433.
58 A. Stroobants, Liquid crystal phase transitions in bidisperse hard-rod systems, *J. Phys.: Condens. Matter*, 1994, **6**, 285.
59 R. Sear and G. Jackson, Theory for the phase behavior of a mixture of a rodlike colloid and a rodlike polymer, *J. Chem. Phys.*, 1995, **103**, 8684–8693.
60 J. Galanis, R. Nossal and D. Harries, Depletion forces drive polymer-like self-assembly in vibrofluidized granular materials, *Soft Matter*, 2010, **6**, 1026–1034.
61 P. de Gennes and J. Prost, *The Physics of Liquid Crystals*, Clarendon, Oxford, 1993.
62 F. Frank, Liquid crystals. On the theory of liquid crystals, *Discuss. Faraday Soc.*, 1958, **25**, 19–28.
63 T. Shimmen and E. Yokota, Cytoplasmic streaming in plants, *Curr. Opin. Cell Biol.*, 2004, **16**, 68–72.
64 D. DeRosier and L. Tilney, F-Actin bundles are derivatives of microvilli, *J. Cell Biol.*, 2000, **148**, 1–6.
65 J. Bartles, Parallel actin bundles and their multiple actin-bundling proteins, *Curr. Opin. Cell Biol.*, 2000, **12**, 72–78.
66 A. Liu, D. Richmond, L. Maibaum, S. Pronk and P. Geissler, Membrane-induced bundling of actin filaments, *Nat. Phys.*, 2008, **4**, 789–793.
67 D. Courson and R. Rock, Actin crosslink assembly and disassembly mechanics for alpha-actinin and fascin, *J. Biol. Chem.*, 2010, **285**, 26350–26357.
68 D. Vignjevic, S. Kojima, Y. Aratyn, O. Danciu, T. Svitkina and G. Borisy, Role of fascin in filopodial protrusion, *J. Cell Biol.*, 2006, **174**, 863–875.
69 A. Reymann, J. Martiel, T. Cambier, L. Blanchoin, R. Boujemaa-Paterski and M. Théry, Nucleation geometry governs ordered actin networks structures, *Nat. Mater.*, 2010, **9**, 827–832.
70 J. Pardee and J. Spudich, Purification of muscle actin, *Methods Enzymol.*, 1982, **85**, 164–181.